JCTC Journal of Chemical Theory and Computation

NMR Relaxation and Internal Dynamics of Ubiquitin from a 0.2 μs MD Simulation

Aart J. Nederveen and Alexandre M. J. J. Bonvin*

Bijvoet Center for Biomolecular Research, Utrecht University, Utrecht, The Netherlands

Received November 19, 2004

Abstract: A 0.2 μs molecular dynamics simulation of ubiquitin in water is presented, which allows us to assess both the global tumbling in solution and the internal dynamics. The latter reveals slow motions outside the classical NMR timewindow, in agreement with recent RDC and cross-correlation measurements. Analysis of back-calculated relaxation rates using the classical NMR model-free approach reproduces the amplitudes of internal motions expressed in the order parameter, while it severely underestimates the corresponding time scales present in the simulation.

I. Introduction

Motion in the picosecond and nanosecond time scale can be monitored in Nuclear Magnetic Resonance (NMR) relaxation studies.[1] Important characteristics of motions in these time scales can be studied with the help of molecular dynamics (MD) simulations. In the past decade significant progress has been made in the assessment of biomolecular NMR data with MD simulations (for a review see ref 2). In many cases, the amplitudes of motions found in MD simulation are in good agreement with the corresponding values derived from experimental data although, in general, the simulated values tend to be somewhat lower. For globular proteins, MD simulations are typically restricted to simulation time lengths of tens of nanoseconds. As a result the global tumbling cannot be sampled and needs to be artificially included when back-calculating NMR parameters. In addition, a proper description of internal motions in the nanosecond to microsecond time scale which are of biological relevance, especially in the context of folding, recognition, and enzymatic function, requires much longer simulation times.

Thanks to the continuously increasing computing power, MD simulations in the microsecond time scale are now within our reach. Duan and Kollman[3] presented a 1 μs MD simulation of a 36-residue peptide (HP-36) starting from an unfolded structure, showing that, within that time period, a marginally stable folded state could be reached. In the context of NMR, simulations in the microsecond time scale have been reported in the literature for small peptides. Feenstra et al.[4] performed several simulations of a nonapeptide in water up to 0.7 μs in an attempt to simulate NMR NOE/ROE intensities. Peter et al.[5] presented two 0.2 μs simulations of a heptapetide of β-amino acids in methanol from which they simulated ROESY spectra by calculating the exact spectral densities for the interproton vectors. In that study the separability of internal and global motions could be confirmed for most of the residues, indicating that the global tumbling of the molecule and the internal motions are uncorrelated. Although this decorrelation assumption underlies many of the standard methods for analyzing NMR relaxation data, its validity for larger proteins has recently been questioned.[2,6] In addition, it has been suggested that time scales in standard NMR relaxation studies are significantly underestimated.[7] Long MD simulations should allow for addressing this question.

In this paper we present the results of two long MD simulations (0.1 and 0.2 μs) of ubiquitin, a well-studied 76 amino acid globular protein. Human ubiquitin is one of the most conserved eukaryotic proteins. Its primary role is in intracellular, ATP-dependent protein degradation.[8] Several sets of NMR data, describing the dynamics of ubiquitin, are available in the literature, including $^{15}N^{1}H$ R_1, R_2, and NOE ratios,[9−11] order parameters derived from residual dipolar couplings (RDCs),[12,13] and cross-correlated relaxation data.[14−16]

* Corresponding author phone: +31.(0)30.2533859; fax: +31.(0)30.2537623; e-mail: a.m.j.j.bonvin@chem.uu.nl. Corresponding author address: Department of NMR Spectroscopy, Bijvoet Center for Biomolecular Research, Utrecht University, Padualaan 8, 3584 CH Utrecht, The Netherlands.

10.1021/ct0498829 CCC: $30.25
Published on Web 03/31/2005

The RDC and cross-correlation data provide evidence for slow motions in the nanosecond to microsecond time scale both in loops and secondary structure elements. Such slow motions are typically not monitored in standard NMR-relaxation analysis.

Our 0.2 μs MD simulation allows us to estimate the global tumbling of ubiquitin in solution and study its internal dynamics, revealing slow motions outside the classical NMR timewindow in agreement with the recent RDC and cross-correlation measurements. The R_1, R_2, and NOE relaxation rates are back-calculated from the spectral densities obtained after Fourier transformation of the internal correlation functions. These rates are then used as input for the classical NMR model-free analysis to check if this commonly used analysis can properly extract the amplitudes and time scales of the internal motions present in our simulation.

II. Materials and Methods

A. Simulations. Two independent trajectories are presented in this paper: a trajectory starting from the refined NMR structure of 1D3Z[17] taken from the DRESS database[18] (NMR trajectory) and a trajectory starting from the first monomer of the dimeric X-ray structure of 1AAR[19] (X-ray trajectory, see Figure 1). The latter trajectory shall be extensively investigated throughout this paper, whereas the former will be used for validation. Simulations and analysis were performed using the GROMACS package,[20] version 3.1.3, with the GROMOS96 43a1 force field.[21]

The solute was placed in a cubic box, with a minimum solute-box distance of 1.4 nm and solvated with SPC waters.[22] No counterions were used since the net charge of the system was zero (neutral pH). The entire system consists of 760 solute atoms and 10 257 and 11 393 water molecules for the X-ray and NMR systems, respectively. A short energy minimization was performed on the system with positional restraints on the protein. Then a MD equilibration stage was carried out consisting of five successive 20 ps runs with decreasing positional restraints force constants on the solute (K_{posre} = 1000, 1000, 100, 10, and 0 kJ mol^{-1} nm^{-2}). After that the production runs were started. For the X-ray trajectory 218 ns were simulated, whereas the total simulation time for the NMR trajectory amounted to 100 ns.

For the integration of the equations of motion a 2 fs time step was used. Positions and velocities were stored every 2 ps. In each simulation the temperature was maintained at 300 K by weakly coupling solute and solvent separately to an external bath using the Berendsen thermostat[23] with a relaxation time of 0.1 ps, whereas the pressure was maintained by weakly coupling the system to an external pressure bath[23] at 1 atm with a coupling constant of $\tau_p = 0.5$ ps. The neighbor list was updated every 10 integration steps. The twin-range method was applied for dealing with long-range interactions, the short-range cutoff being 1.0 nm and the long-range cutoff 1.4 nm, both for electrostatic and van der Waals interactions. Electrostatic interactions beyond the cutoff were treated with a generalized reaction field[24] using a dielectric constant of 54.0.

B. NMR Relaxation Theory. The NMR relaxation theory has been extensively described elsewhere.[25,26] In this paper we focus on the relaxation of the amide ^{15}N nuclear spin through dipolar interaction with the attached ^{1}H spin and ^{15}N Chemical Shift Anistropy (CSA). The relaxation in this case is governed by the correlation function of the ^{15}N-^{1}H spin-interaction vector $\vec{r}(t)$

$$C(t) = \frac{4\pi}{5}\sum_{m=-2}^{m=2}\left\langle \frac{Y_{2m}(\theta_\tau,\phi_\tau)Y_{2m}(\theta_{\tau+t},\phi_{\tau+t})}{r^3(\tau)r^3(\tau+t)}\right\rangle_\tau \quad (1)$$

where Y_{2m} are the second rank spherical harmonics, $r(t)$ is the interaction vector, and (θ_τ, ϕ_τ) is the polar angles of the interaction vector at time τ in the laboratory frame of reference. Using the addition theorem for spherical harmonics, this expression can be rewritten as

$$C(t) = \left\langle \frac{P_2(\cos\chi_{\tau,\tau+t})}{r^3(\tau)r^3(\tau+t)}\right\rangle_\tau \quad (2)$$

where $P_2(x) = {}^3/_2x^2 - {}^1/_2$ is the second-order Legendre polynomial and $\chi_{\tau,\tau+t}$ is the angle between the interaction vectors at times τ and $\tau + t$. Equation 2 is used in this paper for the calculation of the global correlation function for each backbone amide-proton pair from the MD trajectory.

The spectral density function $J(\omega)$ can be obtained by Fourier transformation of the correlation function. According to the relaxation theory of Bloch, Wangness, and Redfield[26] this function is probed at specific frequencies in NMR ^{15}N relaxation experiments for R_1, R_2, and NOE

$$R_1 = \frac{d^2}{4}[3J(\omega_N) + J(\omega_H - \omega_N) + 6J(\omega_H + \omega_N)] + \frac{c^2}{3}J(\omega_N) \quad (3)$$

$$R_2 = \frac{d^2}{8}[4J(0) + 3J(\omega_N) + J(\omega_H - \omega_N) + 6J(\omega_H) + 6J(\omega_H + \omega_N)] + \frac{c^2}{18}[4J(0) + 3J(\omega_N)] \quad (4)$$

$$\mathrm{NOE} = 1 + \frac{d^2}{4R_1}\frac{\gamma_H}{\gamma_N}[6J(\omega_H + \omega_N) - J(\omega_H - \omega_N)] \quad (5)$$

where $d = \mu_0 h\gamma_H\gamma_N r_{NH}^{-3}/8\pi^2$, $c = \Delta\sigma\omega_N$, μ_0 is the permeability of free space, h is Planck's constant, γ_N and γ_H are the gyromagnetic ratios of ^{15}N and ^{1}H nuclei, $\Delta\sigma$ is the CSA of ^{15}N, r_{NH} is the N−H distance, and ω_N and ω_H are the Larmor frequencies of the ^{15}N and ^{1}H nuclei.

From NMR relaxation experiments the values of R_1, R_2, and NOE for nonproline residues can be determined. Two methods are in use for extracting the dynamic information from these rates. Spectral density mapping[29] can be used to directly determine the values of the spectral density functions that are probed by NMR. In this paper reduced spectral density mapping[30] is used for calculating the spectral density values from experimental relaxation data. This approach assumes that $J(\omega_H + \omega_N) = J(\omega_H) = J(\omega_H - \omega_N)$, which is valid if the spectral density function is flat at high frequencies.

The most popular method for analyzing NMR relaxation data of proteins is the Lipari-Szabo model-free approach.[31,32] This approach uses no specific model for describing the

internal motion of the interaction vector. It is based on the decorrelation assumption that splits up the global correlation function in an internal correlation function and the overall correlation function of the molecule:

$$C_{\text{global}}(t) = C_{\text{int}}(t)C_{\text{overall}}(t) \quad (6)$$

In the case of isotropic tumbling $C_{\text{overall}}(t)$ can be taken as e^{-t/τ_c}, where τ_c is the global correlation time, which gives an indication of the tumbling frequency of the protein in the solvent. $C_{\text{int}}(t)$ now describes the internal motion of the NH-interaction vector within the molecular frame of the molecule studied. The model-free analysis yields an order parameter S^2 describing the magnitude of the internal motions along with an estimation of the internal time scale τ_e. Nowadays five models are commonly used within the model-free approach, each of them fitting a specific form of the spectral density function $J(\omega)$ to the experimental data, leading to various combinations of parameters:[33]

- model 1: S^2,
- model 2: S^2,τ_e,
- model 3: S^2,R_{ex},
- model 4: S^2, τ_e, R_{ex}, and
- model 5: S^2_s, S^2_f, τ_s.

R_{ex} indicates conformational exchange on the millisecond and microsecond time scale. Model 5 delivers information on internal motions taking place at slow and fast time scales. Selection of the model that fits best the available experimental data is commonly based on χ^2-statistics and F-tests. In this paper the model-free analysis of back-calculated NMR relaxation data is carried out with the program TENSOR2.[33]

Throughout this paper the following physical constants were used: $\Delta\sigma = -170$ ppm and $r_{NH} = 0.102$ nm. We made use of three different experimental relaxation data sets of ubiquitin measured at 600 MHz, that were reported by Lienin et al.,[9] Fushman et al.,[11] and Lee et al.[10] From these data sets one averaged set was generated consisting of R_1, R_2, and NOE for 62 residues (see Supporting Information). The standard deviations calculated from the 3 different sets are in the same range as the reported experimental errors. This average set was used as input data for the reduced spectral density mapping and for the comparison with the relaxation data from the MD simulation.

C. Analysis of Internal Dynamics. The internal dynamics of ubiquitin is assessed by computing the internal correlation function of the NH-vectors from the MD simulation with eq 2, after superposition of all structures onto the backbone heavy atoms of the secondary structure elements of the starting structure. These comprise the following segments (as defined with the program DSSP[34]): 5 β-sheets (2−7, 12−16, 41−45, 48−49, 66−71) and 1 α-helix (23−34). When the internal correlation function converges, the value of the plateau, $C_{\text{int}}(\infty)$ can be estimated as[35]

$$C_{\text{int}}(\infty) = \frac{4\pi}{5}\sum_{m=-2}^{m=2}|\langle Y_{2m}(\theta,\phi)\rangle|^2 = \frac{1}{2}(3\sum_{i=1}^{3}\sum_{j=1}^{3}\langle\mu_i\mu_j\rangle^2 - 1) \quad (7)$$

where μ_i are the Cartesian coordinates of the normalized internuclear NH-vector in the molecular frame. This expression yields the well-known order parameter S^2 that is frequently used for estimating the magnitude of the internal dynamics in a protein.

For determining if the correlation function of a specific residue has converged we use the following criterion: $|C_{\text{int}}(\infty) - C_{\text{tail}}| < 0.005$ where C_{tail} is the mean value of the tail of the internal correlation function. For the 100 ns MD this tail was taken from 45 to 50 ns, whereas for the 218 ns from 90 to 100 ns[7].

If the internal correlation function converges, the effective internal correlation time τ_{int} for these motions can be determined by integrating the correlation function

$$\tau_{\text{int}} = \frac{1}{C_{\text{int}}(t_{\text{start}}) - C_{\text{int}}(\infty)}\int_{t_{\text{start}}}^{T}(C_{\text{int}}(t) - C_{\text{int}}(\infty))dt \quad (8)$$

where T is the timepoint where the function reaches the plateau value and $t_{\text{start}} = 2$ ps. Autocorrelation functions calculated from MD simulations tend to have a sharp initial drop, that is caused by librational motion of the bonds.[36,37] In calculating τ_{int} we corrected for this initial drop by starting the integration at the first timepoint, thus neglecting the ultrafast motions in the estimation of time scales of the internal motions.

D. Computer Cluster. All calculations were carried out on the TERAS supercomputer, a 1024 CPU system (SGI Origin 3800), at the national computer center SARA (http://www.sara.nl) in Amsterdam, The Netherlands. We used 16 processors in parallel. Per day, approximately 3.5 ns could be simulated if efficient use was made of the available CPU time. Effectively the total cost for both trajectories amounted to approximately 5 months of simulation.

III. Results and Discussion

A. Validation of the Trajectories. Both MD trajectories, the 100 ns one starting from the refined NMR structure (1D3Z[17]), denoted in the following as NMR, and the 218 ns one starting from the crystal structure (1AAR[19]), denoted in the following as X-ray, were validated in terms of secondary structure evolution, RMSD, energetics, and agreement with the experimental NOE data. Both trajectories equilibrated within 1−2 ns. The RMSD relative to the starting structure is presented in Figure 2: both trajectories are stable with the average RMSDs around 0.1 nm for the backbone heavy atoms belonging to secondary structure elements (see also Table 1). Note that the RMSD calculated for residues 2−71 is 0.1 nm lower on average than for the entire backbone (Table 2). This is due to the high flexibility of the C-terminal tail. An increase in the backbone RMSD can be observed in the X-ray simulation between 130 and 185 ns; this increase is due to a change in turn conformation at position 38−41 (also evident in Figure 3). After this event the structure recovers its initial conformation and remains stable until the end of the simulation. The two trajectories sample similar conformational space: the RMSD of one trajectory relative to the starting structure of the other trajectory does not indicate major differences (see Table 1). This is confirmed by an analysis of the pairwise RMSD matrix of the concatenated trajectories: no separate blocks that would indicate conformational differences between the trajectories can be distinguished (see Supporting Information). The RMS

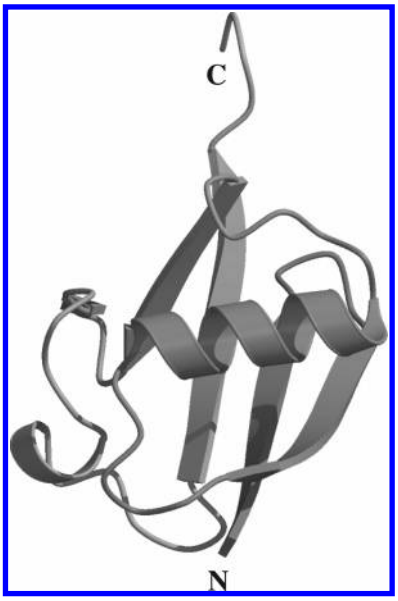

Figure 1. Cartoon representation of ubiquitin (PDB entry 1AAR[19]) showing its secondary structure elements. This figure was generated with Molscript[27] and Raster3D.[28]

fluctuations of the C^{α} atoms exhibit a similar profile for both trajectories (see Figure 2c), except for residues 62−64 that show larger fluctuations in the NMR trajectory and residues 37−39 that have larger fluctuations in the X-ray trajectory.

The time evolution of the secondary structure elements is depicted in Figure 3: in both trajectories the secondary structure is well preserved. In the X-ray trajectory the fourth β-sheet shows some instability in the 155 to 165 ns time interval. The same is observed for the onset of the third β-sheet from 100 ns on. In the time window from 130 to 185 ns there is a change in turn conformation at position 38−41.

Analysis of the energetics of both trajectories does not reveal any major difference (see Table 1).

We further validated our simulation against experimental NMR data by calculating NOE distances using an r^{-6} averaging. We used for this the set of 985 unambiguous distance restraints that are available from the Protein Data Bank[38] for entry 1D3Z.[17] Table 2 summarizes the results of this analysis for both the starting structures and the MD trajectories (see also Supporting Information for NOE violation matrices). In the NMR starting structure (refined 1D3Z from the DRESS database[18]) no violations larger than 0.05 nm are present, and in the NMR-trajectory only 4 restraints are violated by more than 0.05 nm (max. violation 0.16 nm). In the crystal structure (1AAR) 18 restraints are violated by more than 0.05 nm (max. violation 0.21 nm), after adding the protons to the original file, while 13 violations above 0.05 nm are found in the X-ray trajectory (max. violation 0.19 nm). None of the latter are present in the set of 18 violations for the starting structure. Two medium distance restraints, both connecting the helix to the subsequent loop are violated in both trajectories ($31H^{\alpha}$-35H and $30(H^{\gamma 2})_3$-$36H^{\beta}$) by 0.12 nm on average. Considering the very small number of violations, it can be concluded that both trajectories are in excellent agreement with the experimental NOE data.

B. Global Tumbling of the Molecule and Global Correlation Functions. The global tumbling time of the molecule in the solvent is determined by fitting all structures from the trajectory to the backbone heavy atoms of a reference structure, excluding the three highly mobile C-terminal residues. This reference structure was oriented such that its principal axes correspond to the *x*,*y*,*z* axes by calculating the inertia tensor using all heavy atoms excluding the three highly mobile C-terminal residues. Fitting then delivers a rotation matrix for each snapshot from the MD trajectory. The row vectors of the rotation matrix are the rotated unit vectors given in the coordinate system of the reference structure. The correlation functions of these row vectors are plotted in Figure 4a. The global tumbling appears to be much smaller than the experimental value of 4.03 ns.[9] Since the correlation functions are not exponential and not yet fully converged, it is difficult to exactly determine the correlation time for the global tumbling of the molecule from these plots. Integration of the curves yields an average value of 740 ps for the global correlation time. In addition, from this plot it can be concluded that there is a small amount of anisotropy in the global tumbling, since the correlation functions for the different direction are not exactly identical. When taking the estimates for the correlation times τ_1, τ_2, and τ_3 from Figure 4a and using Woessner equations for the

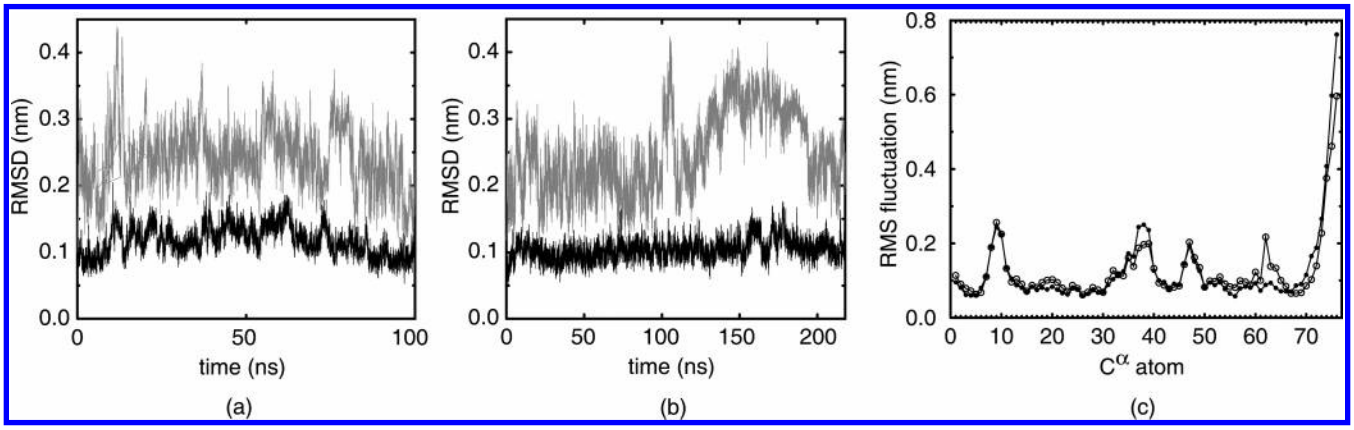

Figure 2. Time evolution of the RMSD relative to the starting structure for the heavy atoms of the entire backbone (grey) and backbone heavy atoms within secondary structure (black): (a) NMR trajectory, (b) X-ray trajectory, and (c) RMS fluctuation of C^{α} positions along the sequence for the NMR trajectory (○) and X-ray trajectory (●).

Table 1. Statistics of the NMR and X-ray MD Trajectories

	NMR	X-ray
heavy atom RMSDs (nm)[a]		
backbone	0.24 (0.05)	0.25 (0.06)
backbone residues 2−71	0.15 (0.02)	0.15 (0.02)
secondary structure	0.12 (0.02)	0.10 (0.02
secondary structure & relative to other[b]	0.12 (0.02)	0.11 (0.03)
Lennard-Jones (van der Waals) energy (kJ/mol)[c]		
ubiquitin internal	−2296 (44)	−2311 (47)
ubiquitin-solvent	−323 (74)	−324 (74)
Coulomb's electrostatic energy (kJ/mol)		
ubiquitin internal	−8966 (237)	−9238 (245)
ubiquitin-solvent	−10418 (486)	−9943 (509)

[a] Positional RMSD values are calculated relative to the starting structure of the trajectories, after superposition onto the secondary structure elements (see Materials and Methods section). Standard deviations are indicated in parentheses. [b] Average RMSDs of the NMR trajectory from the crystal structure and vice versa. [c] The nonbonded energies were calculated with the GROMOS96 43a1 force field using a twin range cutoff of 1.0 and 1.4 nm (see Materials and Methods section). The energies are the sum of short-range and long-range terms.

Table 2. NOE Violation Analysis for 1D3Z, 1AAR, NMR, and X-ray MD Trajectory

	1D3Z[a]	1AAR[b]	NMR trajectory[c]	X-ray trajectory
# violations[d] > 0.05 nm	04	18	4	13
# violations > 0.1 nm	0	7	1	6
maximum violation (nm)	0.02	0.21	0.16	0.19
RMS violations (nm)	0.002	0.017	0.008	0.014

[a] Refined NMR structure of 1D3Z taken from the DRESS database.[18] [b] The crystal structure corresponds to the first unit of the K48-linked ubiquitin dimer. [c] NOE distances in the trajectory are calculated using a r^{-6} averaging. [d] The violation analysis is based on a set of 985 unambigious NOE restraints obtained from the deposited data for entry 1D3Z in the PDB.

principal axis values of the rotational diffusion tensor,[39] we find an experimental value for the anisotropy of the diffusion tensor $D_{\parallel}/D_{\perp}$ of 1.2. The latter value is close to the anisotropy found experimentally: $D_{\parallel}/D_{\perp} = 1.17$.[40]

The discrepancy between the experimental and simulated tumbling times of the molecule in solution can be attributed in part to the SPC water model that is used in our simulation. It is well-known that, while the SPC water model displays good thermodynamic properties, its kinetic properties differ from the experimental values by a factor of 2 to 2.5: its diffusion constant is 5.28×10^{-9} m^2/s against 2.2×10^{-9} m^2/s experimentally and its viscosity is 0.58×10^{-3} Pa·s against 0.85×10^{-3} Pa·s experimentally at 300 K.[41] The fast motions of the water apparently influences the global tumbling of the molecule in the present simulation and possibly also the internal dynamics of exposed regions as will be discussed below. MD simulations using another water model, for example SPC/E, which has better kinetic properties, might lead to better estimates of the overall tumbling. Initials results from a short (10 ns) simulation in SPC/E indeed indicate slower overall tumbling by approximately a factor 2. One should however be aware that this might happen to the detriment of the protein structural stability as it is difficult to find a water model with both excellent thermodynamic and kinetic properties. Note that in another MD simulation using the CHARMM force field[42] similar correlation times in the subnanosecond time range were obtained for the overall tumbling of ubiquitin based on a completely different analysis approach using isotropic reorientational eigenmode dynamics (see Table 1 in ref 43). This indicates that reproducing experimental tumbling times might not be a specific problem related to our choice of force field and analysis methods but rather a more general issue in current biomolecular simulation methodology.

The global ^{15}N-^{1}H correlation functions could be assessed using eq 2. Typical plots for two residues, ASP21 and ALA46, are presented in Figure 4b. These correlation functions converge, although oscillations at longer time scales remain. Direct Fourier transformation of the global correlation functions is now possible to obtain the spectral density function (see inset in Figure 4b). To obtain a smooth spectral density function we use a exponential window function in the time domain ($\exp(-t/a)$, with a set to 8 ns) to remove the remaining long time scale oscillations.

C. Internal Dynamics. The internal dynamics of ubiquitin is assessed by calculating the time correlation functions of the NH-vectors with eq 2, after superposition of all MD snapshots onto the backbone heavy atoms of the secondary structure elements of the starting structure. Using the criterion for the convergence described in the Materials and Methods section, it appears that 50 residues in the 100 ns MD trajectory starting from the NMR structure are not converged, whereas only 20 residues are not converged in the 218 ns trajectory starting from the X-ray structure. Therefore we limit our discussion to the results from the X-ray trajectory. The unconverged residues are as follows: LEU8, THR12, ILE13, GLY35, ILE36, ASP39, GLN40, GLN41, ARG42, LEU43, PHE45, LYS48, GLN49, HIS68, LEU71, ARG72, LEU73, ARG74, GLY75, and GLY76. For these residues the internal dynamics is apparently not yet fully sampled, suggesting the presence of slow motions. Such lack of convergence has often been accounted for by poor sampling of dihedral transitions. Inspection of the time series for the scalar product of the interaction vector $\vec{\mu}(0)\cdot\vec{\mu}(t)$ for the unconverged residues indeed shows jumps that only occur once in the entire simulation window for some of these residues. In Figure 5a four examples of internal correlation functions are presented for short, intermediate, and long time scales together with an example of an unconverged correlation function. The time series of the scalar product for GLY53, ILE44, and GLN40 are shown in insets. Figure 5b

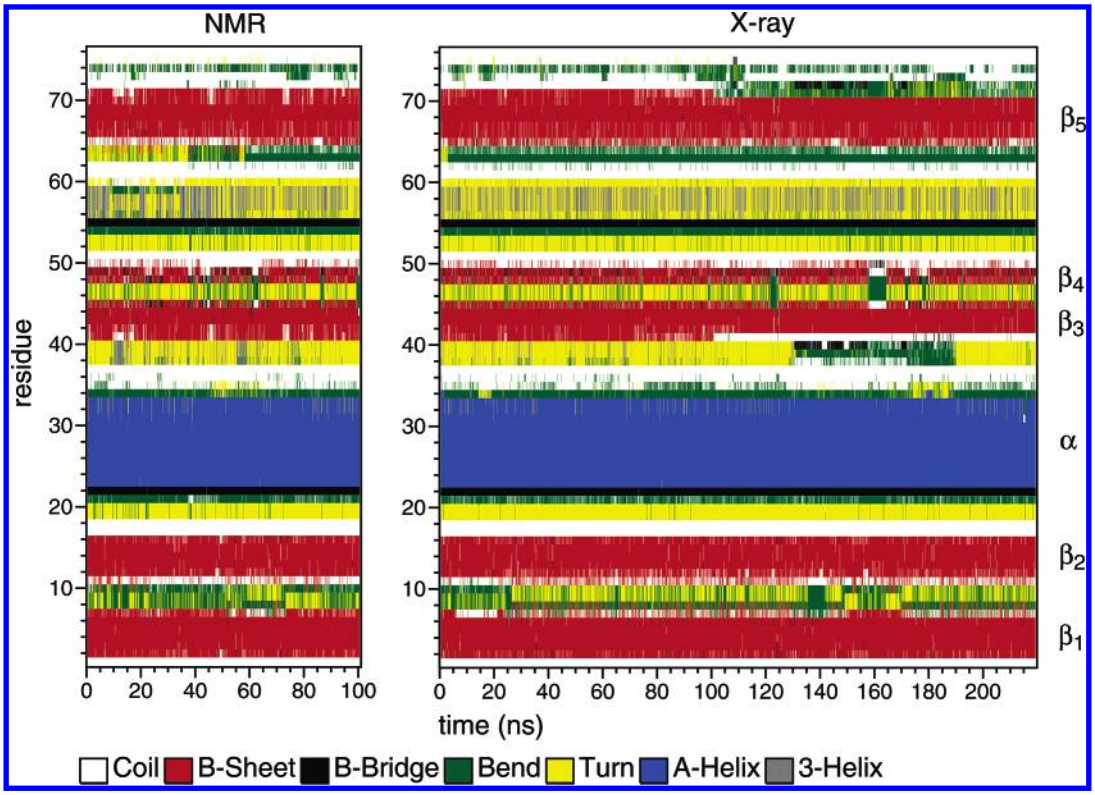

Figure 3. Secondary structure evolution of NMR and X-ray trajectories.

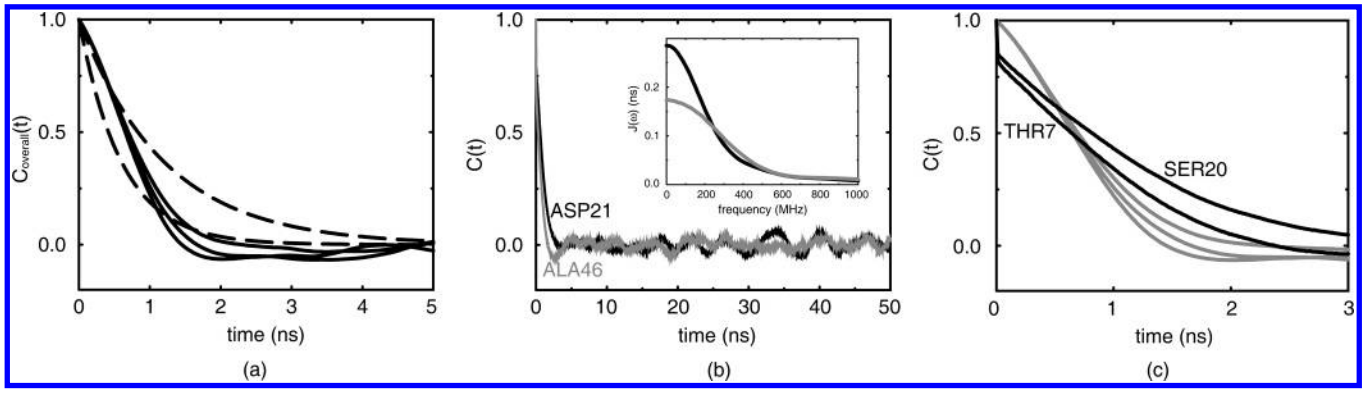

Figure 4. Assessment of global tumbling of the molecule. (a) Overall correlation functions in three directions. Exponential functions ($\exp(-t/\tau_c)$ dashed lines) with $\tau_c = 0.6$ ns and 1.2 ns are plotted for comparison. (b) Global correlation functions for residues ASP21 and ALA46 and their corresponding spectral density functions after Fourier transformation (inset). (c) Global correlation functions (black) for THR7 and SER20, together with overall correlation functions of the molecule (grey, as in panel (a)).

shows the time scales for the internal motions that were calculated using eq 8 for the 52 converging residues. Residues with time scales for the internal dynamics larger than 2 ns are found in the β-turn between the first two β-sheets, between the end of the helix and the third β-sheet and in the fifth β-sheet. Note that by our choice of t_{start} (eq 8) we are neglecting the effect of the ultrafast librational motions and are thus putting the focus on longer time scale motions.

There is no straightforward method for comparing these data with available experimental data. The available RDC order parameters[12,13] for ubiquitin indicate that motions are present beyond the classical NMR relaxation time window. It is however difficult to distinguish specific areas with slower motions. Peti et al.[12] suggested that the deviation between the RDC order parameter and the standard Lipari-Szabo order parameter is most profound in loops and β-sheets, which would partially fit our data. The cross-correlated data[14−16] are more specific than the RDC data but are not necessarily correlated with the mobility of the NH-interaction vectors. However, according to data for cross-correlated dipole−dipole interference between successive $^{13}C^{\alpha}$-$^{1}H^{\alpha}$ vectors, the residues that featured slow local motion mainly reside in the first two β-sheets (2−7, 12, 13) and some residues between (8, 11), in the helix (26, 27, 29, 30) and in the third β-sheet (41−45).[14] Experimental data for cross-correlated chemical shift modulation showed slow motions for residues in the first (7), second (12, 14), third (41, 43), and fifth (66, 68, 69) β-sheet and in the helix (27, 28, 29, 31, 33) and for one residue between the first and second β-sheet (9).[16] Here again there is agreement with our data: the first two β-sheets together with the β-turn between

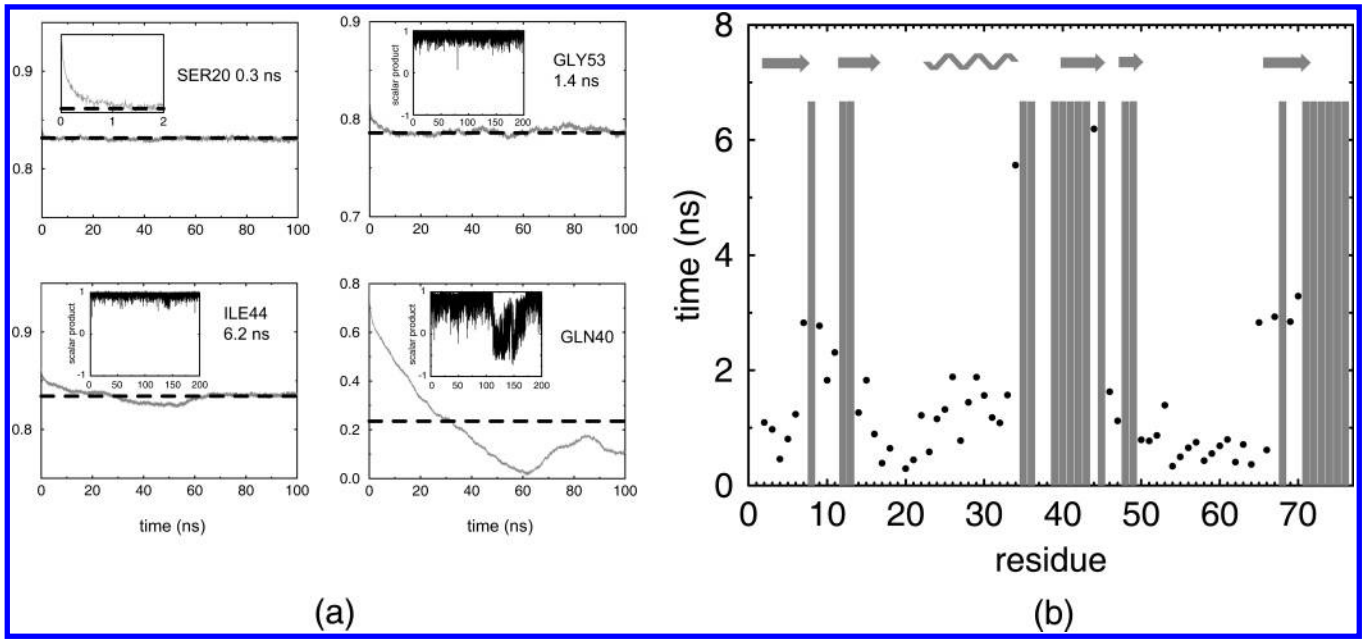

Figure 5. (a) Examples of internal correlation functions: short time scale (SER20), intermediate time scale (GLY53), long time scale (ILE44), and unconverged (GLN40) with $C_{int}(\infty)$ shown as dashed line and (insets) scalar product timeseries of interaction vector for GLY53, ILE44, and GLN40. (b) Correlation times of internal motions for 52 converged residues; unconverged residues are indicated with a gray bar. Secondary structure elements are depicted in top of the figure.

exhibit motions larger than 2 ns, whereas the same applies to the regions 34−45 (end of helix till end of third β-sheet) and 65−70 (fifth β-sheet).

Since we have calculated both the global correlation functions of each residue and the overall correlation function of the molecule, we can now determine if the decorrelation assumption (eq 6) holds for each residue in the present MD simulation. If this equation holds, the global correlation function of a specific residue should not be larger than the overall correlation function of the molecule at any timepoint. We checked this for the first 2 ns for each global correlation function. For 13 residues the global correlation function was larger than the overall correlation function, indicating that for these residues the decorrelation assumption does not hold. This set contains the following residues: THR7, LEU8, THR9, LYS11, THR12, ILE13, SER20, ASP21, PHE45, LYS48, ASP52, GLY53, and GLU64. Some of these residues belong to the residues with long time scale internal motions, indicating that the presence of long time scale motions can be correlated to a failure of the decorrelation assumption. In Figure 4c two examples are shown, THR7 and SER20, for which the decorrelation assumption does not hold.

D. Order Parameters. We can assess the order parameter S^2 calculated from the MD simulation using eq 7 for different timewindows. Figure 6a shows the order parameters calculated for 0.1, 1, 10, and 200 ns timewindows. For the first three cases the order parameter is averaged over all available time windows. For some residues the order parameter decreases with increasing timewindow; these correspond to residues with unconverged correlation functions or long correlation times for the internal motions (see Figure 5b).

In Figure 6b the order parameters derived from the 1 ns timewindow are compared to the experimentally derived order parameters from Lienin et al.[9] Only the 62 residues for which experimental data exists are now considered. The error bars for the MD values were taken as the standard deviation calculated from the averages over the different time windows. Overall the order parameter from the simulation follows the experimental values (correlation coefficient r=0.78), although the MD values are lower on average: 0.74 $\pm$ 0.14 compared to 0.81 $\pm$ 0.13 experimentally. Three residues considerably deviate: LYS11, LYS48, and ARG54, indicating that, in the simulation, those residues have more subnanosecond motions than experimentally derived. These three residues are solvent exposed, preceded by a glycine residue and located outside (LYS11, ARG54) or at the edge (LYS48) of secondary structure elements. Other glycine residues are present at the positions 35, 75, and 76 in the sequence. For GLY35 the deviation from the experimental order parameter is slightly less than in the other cases, possibly due to the fact that this residue is the least solvent exposed from all glycines in the sequence. Here again the overestimation of the amplitude of the fast internal motions may be affected by the too fast dynamics of the water molecules interacting with the protein within the SPC water model.

E. Back-Calculation of NMR Relaxation Data. The spectral density functions were obtained by Fourier transformation of the global correlation functions directly calculated from the MD simulations using eq 2. For comparing the simulated values of the spectral densities at the frequencies $\omega = 0$, ω_N, ω_H with the experimental values, the latter are calculated with the help of reduced spectral density mapping[30] from the averaged experimental set (see Supporting Information). Figure 7 shows the ratios J_{exp}/J_{md} for the frequencies $\omega = 0$, ω_N, ω_H for all residues. It appears that there is a large discrepancy between the simulated and the experimental values, especially at $\omega = 0$ and $\omega = \omega_H$, indicating that there are on average too many fast global motions and too little slow global motions in the simulation. The mean ratio between J_{exp}/J_{md} at $\omega = 0$ is 7.2, which

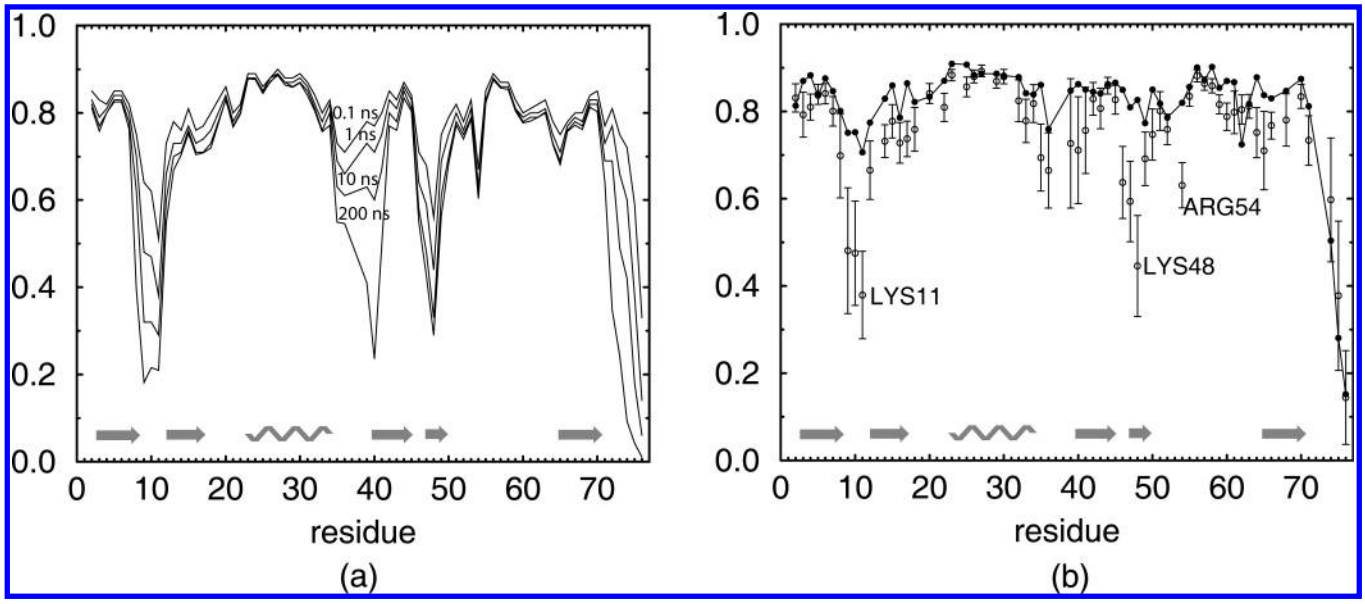

Figure 6. (a) Order parameters profiles for increasing timewindows and (b) comparison of experimental (●) and simulated (○) values averaged over the 1 ns timewindow.

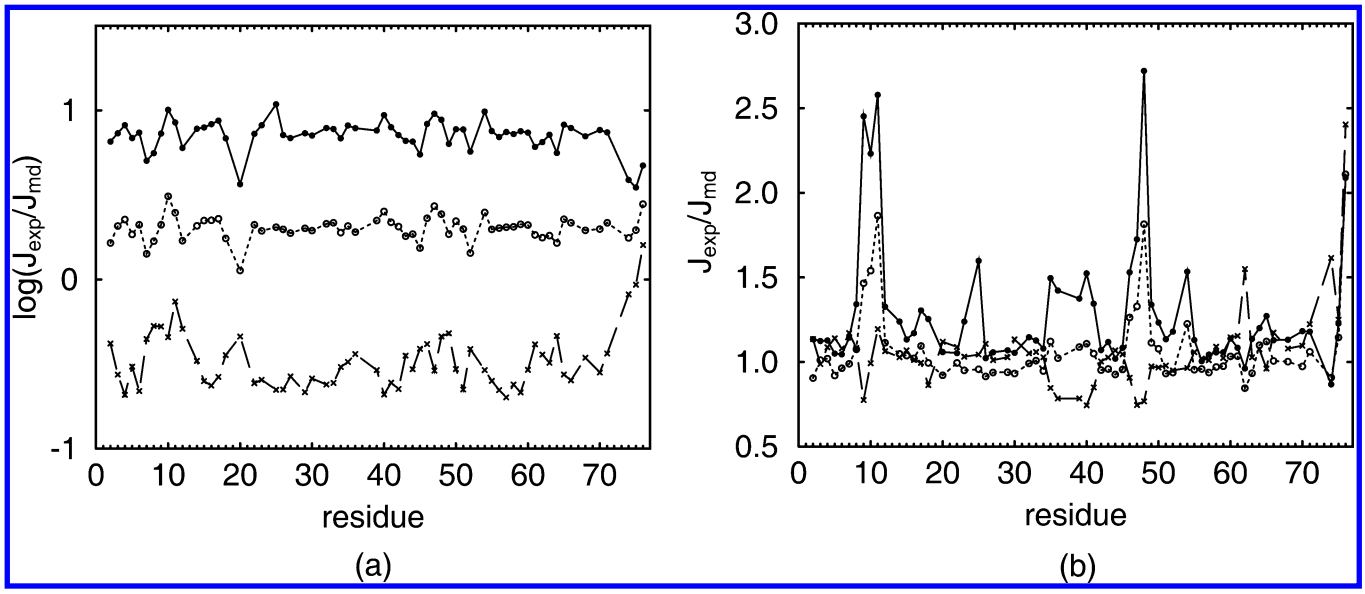

Figure 7. Ratio of spectral densities derived from the MD trajectories and the experimental data at frequencies 0 (●), ω_N (○), and ω_H (×) with (a) global tumbling as present in MD and (b) global tumbling $\tau_c = 4.03$ ns added. Note that the logarithm (base 10) of the ratio is indicated in the left panel (a).

reflects the factor by which the global tumbling is off from the experimental value.

Using eq 6 the global correlation function for each residue is reassessed assuming isotropic tumbling with $\tau_c = 4.03$ ns.[9] The second term in eq 6, $C_{overall}(t)$, thus becomes the isotropic function $\exp(-t/\tau_c)$. The first part is given by the internal correlation functions calculated using eq 2, after superposition of all structures onto the backbone heavy atoms of the secondary structure elements of the starting structure. After Fourier transformation of the resulting global correlation functions for each residue, spectral densities are obtained that are much closer to the experimental values for the spectral density as can be seen from Figure 7b. For both $J(0)$ and $J(\omega_N)$ large deviations are present for THR9, GLY10, LYS11, ALA46, GLY47, LYS48, and to some extent ARG54. The same applies for the segment 35−41. This can be attributed to the increased amplitude of the fast internal motions for those residues (also apparent in Figure 6b for the order parameters) which translates into an overestimation of $J(\omega_H)$ at the expense of $J(0)$ and $J(\omega_N)$ that become smaller since the integral over $J(\omega)$ must remain constant. The deviation of $J(0)$ for ASN25 originates from the large exchange contribution R_{ex} in the experimental data. The other small deviations of the J_{exp}/J_{sim} ratio from 1 may not be significant considering the amount of uncertainty that exists for the physical parameters used[2,37] and the experimental tumbling time.[10] Furthermore, small deviations from 1 may also originate from the anisotropy which is present in the experimental values[40] and which we omitted in our simulated values by assuming isotropic tumbling.

Direct calculation of NMR relaxation data is now feasible by substituting the spectral density values in eqs 3, 4, and 5.

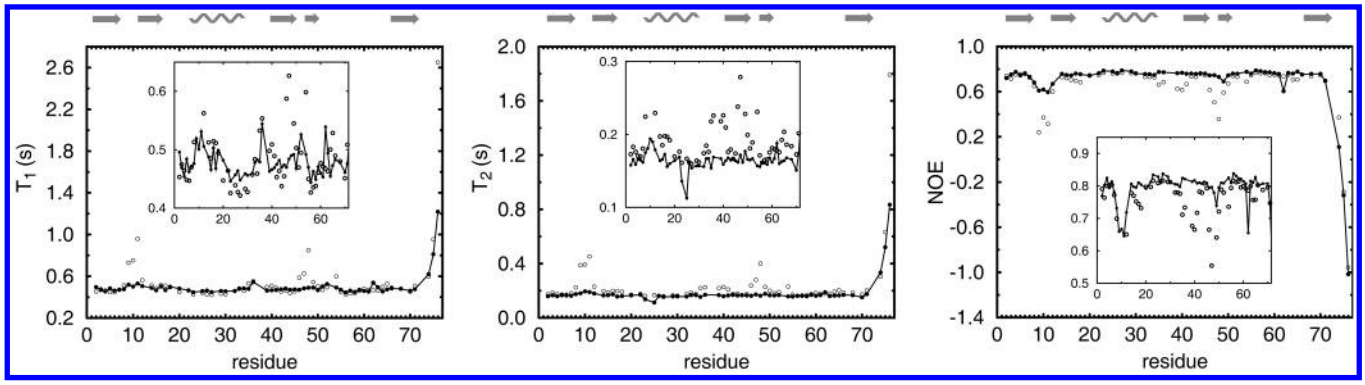

Figure 8. Experimental (●) and simulated (○) NMR relaxation data for T_1, T_2, and NOE. In the insets residues 1−71 are shown; relaxation parameters for residues 9−11 and 48 are off scale.

The quantitative agreement is poor if done for the values in Figure 7a (data not shown) since the global tumbling of the molecule is not reproduced in the simulation. Therefore we used the internal correlation functions from the simulation as before to derive the global correlation functions per residue using eq 6. The agreement now is quite good as can be noticed in Figure 8, although some residues still considerably deviate: 9−11, 35−41, 46−48, and 54. As discussed above, this deviation is mainly due to the presence of fast internal motions in the simulation. These fast motions are visible as the initial rapid decay from $C(0) = 1$ to a lower value. E.g. for LYS11 the value for both the internal and global correlation function is 0.67 at $t = 10$ ps. This indicates that substantial motion is present below this time scale that is responsible for the initial rapid decay of the correlation functions. In Figure 6 the aforementioned residues also deviate from the experimental S^2 values indicating again that too much fast internal motion is present on the subnanosecond time scale. The internal motions in the 2−6 ns range which we presented in Figure 5 do, however, not affect the relaxation data, since they are shielded by the global tumbling of the molecule: for example the T_1, T_2, and NOE values for residues GLU34 and ILE44 for which we found internal correlation times of 5.6 ns and 6.2 ns, respectively, are in good agreement with the experimental data.

F. Model-Free Analysis. Since we now have a complete and consistent picture of the dynamic properties of ubiquitin from our simulation including order parameters S^2, correlation times of internal motions τ_{int}, and predicted R_1, R_2, and NOE data, we can assess the robustness of model-free approaches to extract information on internal dynamics from relaxation data. For this we used the program TENSOR2[33] to extract order parameters and internal time scales from the relaxation data derived from the MD simulation (see Figure 8). We ran TENSOR2 with an experimental uncertainty of 2.5%. This value is a good approximation of the errors that are commonly present in NMR relaxation studies. A minimum absolute uncertainty of 0.01 is used for the NOE values.

We restricted our analysis to 43 residues that fulfilled the following criteria: i) The internal correlation function converges in the MD simulation. ii) The internal correlation time τ_{int} estimated in the MD is smaller than 2 ns. Larger motions are shielded by the global molecular tumbling (as shown above) and can consequently not be reproduced by TENSOR2.

Table 3. Result for Model-Free Analysis of Back-Calculated Relaxation Parameters from MD Trajectory

model	number	τ_{MF}[a]	τ_{int}[b] (ns)	$S_{MF}^2 - S_{MD}^2$
1	33[c]	n/a	0.9 ± 0.5	0.03
2	7[d]	19 ± 5 ps	0.6 ± 0.3	0.01
5	3[e]	1.4 ± 0.1 ns	1.5 ± 0.3	−0.15

[a] Time scales as calculated by TENSOR2. In case model 1 is selected, no time scale is assigned. [b] Internal time scales from MD simulation as calculated by eq 8 and presented in Figure 5. [c] GLN2, PHE4, VAL5, LYS6, THR14, LEU15, SER20, ASP21, THR22, ILE23, GLU24, ASN25, VAL26, LYS27, ALA28, LYS29, ILE30, GLN31, ASP32, LYS33, GLU51, ASP52, GLY53, THR55, LEU56, SER57, ASP58, TYR59, ASN60, ILE61, GLN62, LYS63, THR66. [d] ILE3, GLU16, VAL17, GLU18, LEU50, ARG54, GLU64. [e] GLY10, ALA46, GLY47.

For the selected residues TENSOR chose model 1 in 33 cases, whereas the models 2 and 5 were chosen less often: 7 and 3 times, respectively (see Table 3). This means that for 33 cases TENSOR2 is not capable of detecting the nanosecond time scale internal motion that is present for these residues. The same applies to the 7 residues for which model 2 is selected: the time scales of the internal motions are severely underestimated. Only in the 3 cases where model 5 is selected, the time scales are in agreement with the time scales presented in Figure 5. Note that this behavior is not correlated to the failure of the decorrelation assumption that was found for 13 residues (see above).

The failure of detecting nanosecond time scale motions is mainly due to the noise level in the experimental data: lowering the amount of uncertainty in the experimental data to the unrealistically low value of 0.5% favors the choice of model 5, and consequently motions in the nanosecond time scale are detected. However, such small uncertainties may not be realistic from an experimental point of view. In addition, longer time scale motions for all residues would as well be detected if the analysis was performed exclusively with model 5. This would however not be statistically justified because of the unrealistically high associated errors.

The findings for the time scales presented above are in agreement with results presented by Chen et al.[7] They also find that nanosecond time scale motions can go undetected in the model-free analysis and that the model-free time scales consequently underestimate the effective correlation times.

For the selected residues the order parameter is correctly reproduced, as illustrated in Figure 9. The differences be-

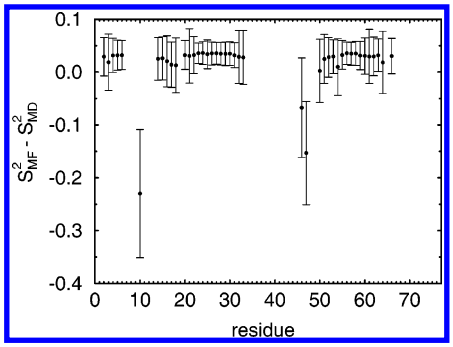

Figure 9. Difference between model-free order parameters (S^2_{MF}) and MD order parameters (S^2_{MD}). Errorbars are calculated as the square root of the quadratic sum of the individual errors.

tween the order parameters predicted by TENSOR2 S_{MF}^2 and the simulated order parameters S_{MD}^2 for the time window of 1 ns are close to zero, except for GLY10 and GLY47 (see Figure 6a). For these residues the predicted order parameters by TENSOR2 are close to the ones calculated for a 10 ns time window. For the residues fitted with model 1 the order parameter is slightly overestimated by an amount of 0.03 (see Table 3), although this difference is not significant for each of the residues (see errorbars in Figure 9).

IV. Conclusions

The present results from our molecular dynamics simulation of ubiquitin allows us to draw several conclusions. Most importantly we have shown that long MD simulations can yield insight in the internal dynamics beyond the time scale that is commonly studied in NMR relaxation studies. Motions on longer time scales than the overall tumbling do not affect the back-calculated NMR relaxation parameters T_1, T_2, and NOE and will consequently go undetected in the standard model-free analysis. We also have shown that time scales are in general underestimated in the standard model-free analysis, unless extremely precise experimental data can be recorded. Consequently nanosecond time scale motions often remain undetected. The observation of slow motions in the present simulation is corroborated by recent experimental studies on protein backbone motion based on residual dipolar coupling measurements and cross-correlation measurements.

One of the generally accepted assumptions that overall and internal motions are uncorrelated in globular proteins,[2] a requisitive for the model-free analysis, does not hold for quite a number of residues in our simulation. Here it should be noted that in the present simulation for many residues the internal correlation time is larger than the global correlation time. This situation is opposite from what is believed to be the case for globular proteins studied with NMR.[2] It remains thus undecided if global and internal motions can be split up following eq 6. Although this relation is widely used in the NMR field, evidence from simulation or experiment that it really holds is sparse.[2,6] To really test this assumption for globular proteins, longer MD simulations of at least 1 μs are needed.

An important point in extending the time scales of MD simulations for this purpose is that suitable parameters and solvent models should be used that reproduce the overall tumbling in solution. Most force fields, however, have been parametrized on much shorter time scales aiming at properly reproducing structural, short time scale dynamics, and thermodynamics properties. Obtaining parameters that, in addition, properly reproduce long time scale dynamics and overall tumbling remains a challenge. Such an effort will also strongly depend on the availability of high quality experimental data describing long time scale dynamics in biomolecules.

In conclusion, the present work underlines both the strengths and weaknesses of MD simulation methods and, to some extent, the experimental limitations of NMR relaxation studies, especially regarding the required accuracy, in properly describing long times scale dynamics.

Acknowledgment. We thank Dr. Chris Spronk (Radboud University) for providing us with the refined model of 1D3Z. Dr. Rafael Brüschweiler (Clark University) and Dr. David Fushman (University of Maryland) are acknowledged for providing their experimental relaxation data of ubiquitin. Rafael Brüschweiler, Martin Blackledge (IBS Grenoble), Jeanine Prompers (Eindhoven University), Klaartje Houben (Utrecht University), Hans Wienk (Utrecht University), and Christine Peter (NIH) are thanked for useful discussions. Aalt-Jan van Dijk (Utrecht University) is acknowledged for preparing Figure 1. David Fushman is thanked for careful reading of the manuscript. This work was supported by the European Community program NMRQUAL (contract number QLG2-CT-2000-0313).

Supporting Information Available: Cross-RMSD matrix, matrix for NOE violations, and averaged NMR relaxation data set (Table S1). This material is available free of charge via the Internet at http://pubs.acs.org.

References

(1) Bruschweiler, R. New approaches to the dynamic interpretation and prediction of NMR relaxation data from proteins. *Curr. Opin. Struct. Biol.* **2003**, *13*, 175−183.

(2) Case, D. A. Molecular dynamics and NMR spin relaxation in proteins. *Acc. Chem. Res.* **2002**, *35*, 325−331.

(3) Duan, Y.; Kollman, P. A. Pathways to a protein folding intermediate observed in a 1-microsecond simulation in aqueous solution. *Science* **1998**, *282*, 740−744.

(4) Feenstra, K. A.; Peter, C.; Scheek, R. M.; van Gunsteren, W. F.; Mark, A. E. A comparison of methods for calculating NMR cross-relaxation rates (NOESY and ROESY intensities) in small peptides. *J. Biomol. NMR* **2002**, *23*, 181−194.

(5) Peter, C.; Daura, X.; van Gunsteren, W. F. Calculation of NMR-relaxation parameters for flexible molecules from molecular dynamics simulations. *J. Biomol. NMR.* **2001**, *20*, 297−310.

(6) Tugarinov, V.; Liang, Z.; Shapiro, Y. E.; Freed, J. H.; Meirovitch, E. A structural mode-coupling approach to 15N NMR relaxation in proteins. *J. Am. Chem. Soc.* **2001**, *123*, 3055−3063.

(7) Chen, J.; Brooks, C. L. R.; Wright, P. E. Model-free analysis of protein dynamics: assessment of accuracy and model selection protocols based on molecular dynamics simulation. *J. Biomol. NMR* **2004**, *29*, 243−257.

(8) Joazeiro, C. A. P.; Hunter, T. BIOCHEMISTRY: Ubiquitination-More Than Two to Tango. *Science* **2000**, *289*, 2061−2062.

(9) Lienin, S. F.; Bremi, T.; Brutscher, B.; Brüschweiler, R.; Ernst, R. R. Anisotropic intramolecular backbone dynamics of ubiquitin characterized by NMR relaxation and MD computer simulation. *J. Am. Chem. Soc*. **1998**, *120*, 9870−9879.

(10) Lee, A. L.; Wand, A. J. Assessing potential bias in the determination of rotational correlation times of proteins by NMR relaxation. *J. Biomol. NMR* **1999**, *13*, 101−112.

(11) Fushman, D.; Varadan, R.; Assfalg, M.; Walker, O. Determining domain orientation in macromolecules by using spin-relaxation and residual dipolar coupling measurements. *Prog. NMR Spectrosc*. **2004**, *44*, 189−214.

(12) Peti, W.; Meiler, J.; Bruschweiler, R.; Griesinger, C. Model-free analysis of protein backbone motion from residual dipolar couplings. *J. Am. Chem. Soc*. **2002**, *124*, 5822−5833.

(13) Tolman, J. R. A novel approach to the retrieval of structural and dynamic information from residual dipolar couplings using several oriented media in biomolecular NMR spectroscopy. *J. Am. Chem. Soc*. **2002**, *124*, 12020−12030.

(14) Fruh, D.; Tolman, J. R.; Bodenhausen, G.; Zwahlen, C. Cross-correlated chemical shift modulation: a signature of slow internal motions in proteins. *J. Am. Chem. Soc*. **2001**, *123*, 4810−4816.

(15) Deschamps, M.; Bodenhausen, G. Anisotropy of rotational diffusion dipole−dipole cross-correlated NMR relaxation and angles between bond vectors in proteins. *Chem. Phys. Chem*. **2001**, *8/9*, 539−543.

(16) Vugmeyster, L.; Perazzolo, C.; Wist, J.; Frueh, D.; Bodenhausen, G. Evidence of slow motions by cross-correlated chemical shift modulation in deuterated and protonated proteins. *J. Biomol. NMR* **2004**, *28*, 173−177.

(17) Cornilescu, G.; Marquardt, J. L.; Ottiger, M.; Bax, A. Validation of protein structure from anisotropic carbonyl chemical shifts in a dilute liquid crystalline phase. *J. Am. Chem. Soc*. **1998**, *120*, 6836−6837.

(18) Nabuurs, S. B.; Nederveen, A. J.; Vranken, W.; Doreleijers, J. F.; Bonvin, A. M. J. J.; Vuister, G. W.; Vriend, G.; Spronk, C. A. E. M. DRESS: a database of REfined solution NMR structures. *Proteins* **2004**, *55*, 483−486.

(19) Cook, W. J.; Jeffrey, L. C.; Carson, M.; Chen, Z.; Pickart, C. M. Structure of a diubiquitin conjugate and a model for interaction with ubiquitin conjugating enzyme (E2). *J. Biol. Chem*. **1992**, *267*, 16467−16471.

(20) Berendsen, H. J. C.; van der Spoel, D.; van Drunen, R. GROMACS: A message-passing parallel molecular dynamics implementation. *Comp. Phys. Comm*. **1995**, *91*, 43−56.

(21) Daura, X.; Mark, A. E.; van Gunsteren, W. F. Parametrization of aliphatic CHn united atoms of GROMOS96 force field. *J. Comput. Chem*. **1998**, *19*, 535−547.

(22) Berendsen, H. J. C.; Postma, J. P. M.; Van Gunsteren, W. F. In *Intermolecular forces*; Reidel Publishing Company: Dordrecht, Interactions models for water in relation to protein hydration, 1981; pp 331−342.

(23) Berendsen, H. J. C.; Postma, J. P. M.; Van Gunsteren, W. F.; Di Nola, A.; Haak, J. R. Molecular dynamics with coupling to an external bath. *J. Chem. Phys*. **1984**, *81*, 3684−3690.

(24) Tironi, I. G.; Sperb, R.; Smith, P. E.; Van Gunsteren, W. F. A generalized reaction field method for molecular-dynamics simulations. *J. Chem. Phys*. **1995**, *102*, 5451−5459.

(25) Wüthrich, K. *NMR of Proteins and Nucleic Acids*; John Wiley & Sons: New York, 1986.

(26) Cavanagh, J.; Fairbrother, W. J.; Palmer III, A. G.; Skelton, N. J. *Protein NMR Spectroscopy, Principles & Practice*; Academic Press: San Diego, CA, 1996.

(27) Kraulis, P. J. MOLSCRIPT: a program to produce both detailed and schematic plots of protein structures. *J. Appl. Crystallogr*. **1991**, *24*, 946−950.

(28) Merrit E. A.; Murphy M. E. P. Rasterd3D, Version 2.0: a program for photorealistic molecular graphics. *Acta Crystallogr*. **1994**, *D50*, 869−873.

(29) Peng, J. W.; Wagner, G. Mapping of the spectral densities of N−H bond motions in Eglin-C using heteronuclear relaxation experiments. *Biochemistry* **1992**, *31*, 8571−8586.

(30) Farrow, N. A.; Zhang, O.; Szabo, A.; Torchia, D. A.; Kay, L. E. Spectral density function mapping using 15N relaxation data exclusively. *J. Biomol. NMR* **1995**, *6*, 153−162.

(31) Lipari, B.; Szabo, A. Model-free approach to the interpretation of nuclear magnetic resonance relaxation in macromolecules. 1. Theory and range of validity. *J. Am. Chem. Soc*. **1982**, *104*, 4546−4559.

(32) Lipari, B.; Szabo, A. Model-free approach to the interpretation of nuclear magnetic resonance relaxation in macromolecules. 2. Analysis of experimental results. *J. Am. Chem. Soc*. **1982**, *104*, 4559−4570.

(33) Dosset, P.; Hus, J. C.; Blackledge, M.; Marion, D. Efficient analysis of macromolecular rotational diffusion from heteronuclear relaxation data. *J. Biomol. NMR* **2000**, *16*, 23−28.

(34) Kabsch, W.; Sander, C. Dictionary of protein secondary structure: pattern recognition of hydrogen-bonded and geometrical features. *Biopolymers* **1983**, *22*, 2577−2637.

(35) Henry, E. R.; Szabo, A. Influence of vibrational motion on solid-state line shapes and NMR relaxation. *J. Chem. Phys*. **1985**, *82*, 4753−4761.

(36) Fushman, D.; Ohlenschlager, O.; Ruterjans, H. Determination of the backbone mobility of ribonuclease T1 and its 2′GMP complex using molecular dynamics simulations and NMR relaxation data. *J. Biomol. Struct. Dyn*. **1994**, *11*, 1377−1402.

(37) Pfeiffer, S.; Fushman, D.; Cowburn, D. Simulated and NMR-derived backbone dynamics of a protein with significant flexibility: a comparison of spectral densities for the beta ARK1 PH domain. *J. Am. Chem. Soc*. **2001**, *123*, 3021−3036.

(38) Berman, H. M.; Westbrook, J.; Feng, Z.; Gilliland, G.; Bhat, T. N.; Weissig, H.; Shindyalov, I. N.; Bourne, P. E. The Protein Data Bank. *Nucleic Acids Res*. **2000**, *28*, 235−242.

(39) Woessner, D. E. Nuclear spin relaxation in ellipsoids undergoing rotational Brownian motion. *J. Chem. Phys*. **1962**, *37*, 647−654.

(40) Tjandra, N.; Feller, S. E.; Pastor, R. W.; Bax, A. Rotational diffusion anisotropy of human ubiquitin from ^{15}N NMR relaxation. *J. Am. Chem. Soc*. **1995**, *117*, 12562−12566.

(41) Smith, P. E.; Van Gunsteren, W. F. The viscosity of SPC and SPC/E water at 277 and 300 K. *Chem. Phys. Lett*. **1993**, *215*, 315−318.

(42) MacKerell, A. D.; Bashford, D.; Bellott, M.; Dunbrack, R. L.; Evanseck, J. D.; Field, M. J.; Fischer, S.; Gao, J.; Guo, H.; Ha, S.; Joseph-McCarthy, D.; Kuchnir, L.; Kuczera, K.; Lau, F. T. K.; Mattos, C.; Michnick, S.; Ngo, T.; Nguyen,

D. T.; Prodhom, B.; Reiher, W. E.; Roux, B.; Schlenkrich, M.; Smith, J. C.; Stote, R.; Straub, J.; Watanabe, M.; Wi?rkiewicz-Kuczera, J.; Yin, D.; Karplus, M. All-Atom Empirical Potential for Molecular Modeling and Dynamics Studies of Proteins. *J. Phys. Chem. B* **1998**, *102*, 3586−3616.

(43) Prompers, J. J.; Bruschweiler, R. General framework for studying the dynamics of folded and nonfolded proteins by NMR relaxation spectroscopy and MD simulation. *J. Am. Chem. Soc*. **2002**, *124*, 4522−4534.

CT0498829